Phase evolution in the mechanochemical synthesis of stabilized nanocrystalline $(ZrO_2)_{0.97}(Y_2O_3)_{0.03}$ solid solution by PAC technique

Nicolás M. Rendtorff[a,b,c,*], Gustavo Suárez[a,b,d], Esteban F. Aglietti[a,b,d], Patricia C. Rivas[d,e,f], Jorge A. Martinez[c,f]

[a]Centro de Tecnología de Recursos Minerales y Cerámica (CETMIC): (CIC-CONICET-CCT La Plata) Argentina, Camino Centenario y 506. C.C.49, M.B. Gonnet., Buenos Aires B1897ZCA, Argentina
[b]Departamento de Quimica, Facultad de Ciencias Exactas—UNLP, Argentina
[c]CIC-PBA, Buenos Aires, Argentina
[d]CONICET, Buenos Aires, Argentina
[e]Facultad de Ciencias Agrarias y Forestales, UNLP, La Plata, Argentina
[f]Departamento de Física, IFLP, Facultad de Ciencias Exactas, UNLP, La Plata, Argentina

Abstract

The mechanochemical activation process has proved to be an effective technique to enhance a solid-state reaction at relatively low temperatures. In such a process, the mechanical effects of milling, such as reduction of particle size and mixture homogenization, are accompanied by chemical effects. The actual chemical phases during the mechanical treatments are sometimes difficult to identify and quantify at an atomic level. In the present paper the XRD and PAC techniques are used to study the phase content evolution during the milling process to obtain the tetragonal stabilize $(ZrO_2)_{0.97}(Y_2O_3)_{0.03}$ solid solution. It has been determined that 10 min of milling time are enough to start the solid solution formation. Both techniques allowed establishing that the obtained crystalline phase was tetragonal. PAC results showed that the stabilized solid solution occurs via the formation of distorted monoclinic ZrO_2 form not distinguished by XRD. The time evolution of the phase contents could be modeled as a consecutive first order solid state reaction $m\text{-}ZrO_2 \rightarrow m'\text{-}ZrO_2 \rightarrow t\text{-}SS$. The values of the kinetic constants indicate that the process was controlled by the second reaction.
© 2012 Elsevier Ltd and Techna Group S.r.l. All rights reserved.

Keywords: A. Milling; Phase transformation; Perturbed angular correlations; Zirconia

1. Introduction

Pure ZrO_2 appears in three different polymorphs: monoclinic (m-), tetragonal (t-) and cubic (c-) being m-ZrO_2 the thermodynamically stable phase at room temperature (RT). Tetragonal and cubic structures at RT are commonly obtained using solid state thermal treatments to form a solid solution (SS) with metallic cations (Y^{+3}, Ca^{+2}, Mg^{+2}, etc.).

It is well known that the addition of certain amounts of appropriate metal oxide enhances mechanical and thermal properties of zirconia based ceramics. In fact, it causes the stabilization of the meta-stable phases (t- and c-) avoiding the deleterious cracking inherent to the volume change during the t- to m- transition on cooling. As it is known, the doping process with oxides of lower-valent cations such as Y_2O_3, generates oxygen vacancies as compensating charges. Vacancies are highly mobile and are responsible for the ionic conductivity at elevated temperatures in many stabilized zirconia ceramics. The reasons for the appearance of $t\text{-}ZrO_2$ at RT have been investigated intensively. There are several proposed models that emphasize the stabilizing influence of the crystallite size [1,2], lattice strains [3], anionic impurities [4], structural similarities between the starting material and $t\text{-}ZrO_2$ product [5] or lattice defects (oxygen vacancies) [6,7].

---

*Corresponding autor. Tel.: +54 221 4840247; fax: +54 221 4710075.
E-mail address: rendtorff@cetmic.unlp.edu.ar (N.M. Rendtorff).

Stabilized zirconia can be prepared by solid state reaction between the oxides at high temperatures ($> 1400 \,^{\circ}\text{C}$). Co-precipitation and sol-gel methods have also been developed. However, additional thermal ;treatments are required to produce solid solutions with high-temperature structures making it difficult to control microstructural characteristics. For this reason, the development of processes to obtain these phases in milder conditions than those required by conventional methods is of particular importance; for example routes with lower temperature thermal treatments or like in this case without a posterior thermal treatment. That's the reason why mechanochemical activation offers interesting possibilities for the synthesis of these materials at temperatures lower than those used in conventional processing, and for the control of their physicochemical and microstructural properties [8].

The mechanochemical activation process has proved to be an effective technique to enhance a solid-state reaction at relatively low temperatures [9,10] included RT. In this process, the "mechanical" effects of milling namely the reduction of particle size and the mixture homogenization [11,12], are accompanied by chemical effects such as partial decomposition of salts or hydroxides [13,14], resulting in very active reactants with high surface energy.

The results of recent investigation of the mechanochemical synthesis of inorganic nanoparticles have demonstrated that, by selecting suitable chemical reaction paths, stoichiometry of starting materials and milling conditions, the method can be used to synthesize a wide range of nanocrystalline particles [15]. In addition, this method has advantages over other methods of producing nanoparticles in terms of low cost, small particle sizes, low agglomeration, narrow size distributions and uniformity of crystal structure and morphology.

The influence of the milling medium (corundum, agate, stainless steel) on the structural and microstructural changes in m-ZrO_2 has been examined [7]. It was shown that regardless of the type of milling assembly, a small amount of tetragonal t-ZrO_2 appeared when m-ZrO_2 was ball-milled for 3 h or more. The onset of m-$ZrO_2 \rightarrow$ t-ZrO_2 transition occurred only in the products ball-milled with stainless steel assembly and resulted in a complete transition after 20 h of milling. Further ball-milling caused a decrease of the t-ZrO_2 lattice parameters followed by a probable transition into cubic c-ZrO_2 structure. The stabilization of t- and c-ZrO_2 in a product milled with stainless steel assembly can be attributed to the incorporation of aliovalent cations (Fe^{2+}, Fe^{3+} or Cr^{3+}) introduced into the sample due to the wear and oxidation of the milling media.

Zirconia stabilization assisted by high energy ball-milling using calcium and zinc oxide dopants did not show any sign of zirconia stabilization after different ball milling times and that only after thermal treatments cubic zirconia was obtained [16]. Similar results were obtained for the La^{+3}-ZrO_2 solid solutions [8] when the cation contents were within the tetragonal-cubic limit.

In many of the mechanochemical processing studies, previous and/or posterior, chemical and/or thermal treatments are

reported to be needed [15–20]. Nevertheless, the mechanochemical stabilization and sintering of nanocrystalline the $(ZrO_2)_{0.97}(Y_2O_3)_{0.03}$ solid solution from pure oxides [21], suggests that additional processing can be minimized by using high energy milling.

Details of the atomic arrangements of materials of technological uses were studied using short range methods as extended X-ray absorption fine structure (EXAFS) [22] and the perturbed angular correlations (PAC) [23,24] techniques. In particular, PAC technique has proved to be an efficient tool in the investigation of the milling effect of the monoclinic zirconia by showing the quadrupole interactions of special atomic arrays through which the monoclinic phase transforms into the tetragonal form [25].

The aim of the present work is to accurately identify and characterize the resulting phases during the formation of the $(ZrO_2)_{0.97}(Y_2O_3)_{0.03}$ solid solution (SS) while processing nanocrystalline powders by high energy milling (HEM) at room temperature. The evolution of the system as a function of the milling time is modeled by assuming an activation kinetic mechanism.

2. Experimental procedure

2.1. Starting materials

Commercial powders were used as principal raw materials: monoclinic zirconia (m-ZrO_2) (CZ-5 SEPR, France $ZrO_2 + HfO_2 \geq 99.5$; $D_{50} = 0.5 \,\mu\text{m}$) was used together with Yttrium oxide (Y_2O_3) (5600-Molycorp, USA 99.99% $D_{50} = 3 \,\mu\text{m}$).

Fine particle mixtures (0.97 M of m-ZrO_2 and 0.03 M Y_2O_3) were prepared in ethanol in order to achieve an intimate blend and then evaporated at $60 \,^{\circ}\text{C}$ for 24 h.

2.2. Milling conditions

High energy milling (HEM) was performed in an oscillating mill (Herzog HSM-100 with a frequency of $12.5 \, s^{-1}$) during preset times up to 60 min using batches of 20 g. This device operates through the friction and impact caused by the relative movement of a (W-Fe) steel ring and a concentric cylinder placed within a case containing the material to be ground. The samples were milled at different times and identified as Z0 (without milling) Z5, Z10, Z20 and Z60; the number indicating the milling time in minutes.

2.3. Powder characterizations.

Resulting crystalline phases were analyzed by X-ray diffraction (XRD) (Philips 3020 equipment with Cu-K_{α} radiation in Ni filter at 40 kV - 20 mA). The apparent crystallite sizes of monoclinic zirconia and zirconia solid solution (SS) in the milled mixtures were calculated from X-ray diffraction data through the Scherrer equation using the strongest diffraction peaks of planes (1 1 1) for m-ZrO_2

and plane (1 0 1) for SS-ZrO_2. XRD machine calibration in peak broadening was performed using the strongest (1 0 1) plane diffraction line of well-crystallized quartz for crystallite size calculation.

The volume fractions of the m-ZrO_2 and t-ZrO_2 (V_m and V_t) were obtained from the integral intensities (I) of the monoclinic diffraction lines (1 1 1) and ($\bar{1}$ 1 1) and the tetragonal diffraction line (1 0 1), following a procedure proposed by Toroya et al. [26]. The volume fractions are given by the following equations:

$$V_t = 1 - V_m \tag{1}$$

$$V_m = \frac{1.311x}{1 + 0.311x} \tag{2}$$

$$x = \frac{I_m(\bar{1}11) + I_m(111)}{I_m(\bar{1}11) + I_m(111) + I_t(101)} \tag{3}$$

The specific surface area of the powders was measured by BET gas adsorption using a Micromeritics Gemini 2360 Surface Area Analyzer.

Finally in order to estimate the lattice parameters of the SS produced during the milling treatment, the XRD patterns were analyzed with the program FullProf, which is a multipurpose profile-fitting program, including Rietveld refinement [27,28].

2.4. PAC analysis

Natural zirconium contains 1–5% of hafnium impurities randomly distributed at zirconium sites. The PAC method [29] makes profit of these impurities to probe the electric field gradient (EFG) V_{ij} produced by the charge distribution at its nearest environment. On account of the r^{-3} dependence of the EFG, the technique probes short range behaviors. The EFG interacts with the quadrupole moment Q of the 482 keV nuclear state ($I = 5/2^+$) of ^{181}Ta, obtained from β^- decay of ^{181}Hf, perturbing the direction of the nuclear radiations emitted. The ^{181}Hf isotope is obtained by irradiating a small amount of the sample (~ 70 mg) with thermal neutrons and the perturbing function which describes the hyperfine quadrupole interaction EFG-Q is known, from the PAC theory, as the spin rotation curve $A_2G_2(t)$:

$$A_2G_2(t) = A_2[\sigma_{20}(\eta) + \sum_{n=1}^{3} \sigma_{2n}(\eta) \ e^{-\delta \ \omega_n \ t} \ \cos(\omega_n t)] \tag{4}$$

where A_2 is a constant which depends on the nuclear spins involved in the emission, the ω_n transition frequencies are already known functions of the quadrupole frequency $\omega_Q \propto V_{ZZ}$ (V_{ZZ}: EFG's major component) and of the asymmetry parameter $\eta = \frac{V_{xx} - V_{yy}}{V_{zz}}$. The σ_{2n} are coefficients that depend on the asymmetry parameter η. In addition, the degree of local disorder often associated to the presence of lattice defects can be taken into account through the distribution width or spread δ of the hyperfine quadrupole frequency.

Whenever the probes of a certain sample are occupying nonequivalent sites, the situation is described considering a linear superposition of perturbation factors $G_2^i(t)$ as defined in Eq. (2):

$$G_2^*(t) = \sum_i f_i G_2^i(t) \tag{5}$$

The f_i coefficients, called population, are considered as the relative abundance of each interaction.

PAC measurements were performed using a four BaF_2 detectors setup with a time resolution of about 1 ns at ^{181}Hf energies.

3. Results and discussion

Fig. 1 displays the XRD patterns of the powders after different milling times (Z0, Z5, Z10, Z20 and Z60). Z0 sample showed as expected peaks of the m-ZrO_2 accompanied by the principal diffraction peak of the Y_2O_3 at $2\theta = 29.24$. This peak was not detected in the milled samples Z5, Z10, Z20 and Z60 but instead the appearance of a broad peak at around 30.4° was observed (see detail) which was attributed to the $(ZrO_2)_{0.97}(Y_2O_3)_{0.03}$ solid solution (SS) formation. Table 1 shows the results obtained by performing a simple quantification following Toroya et al. [26]. The m-ZrO_2 is gradually replaced by the solid solution.

Fig. 2 shows the specific area evolution and the crystallite size determined in the different samples as a function of milling time. The specific surface area increase (by a factor of three) up to 10 min of milling time can be seen, after which a noticeable reduction is determined. The milling processes produced agglomeration of particles with high superficial energy already observed by SEM in a previous work [21].

Regarding crystallinity, as shown in Fig. 2, HEM clearly influenced on the crystallite size ε of the m-ZrO_2. In fact, the initial 55 nm crystallite size ε decreases to ≈ 15 nm after 10 min of milling. The decreasing rate at longer milling times seems to be slower. On the other hand the crystallite size of the mechano-chemically stabilized SS
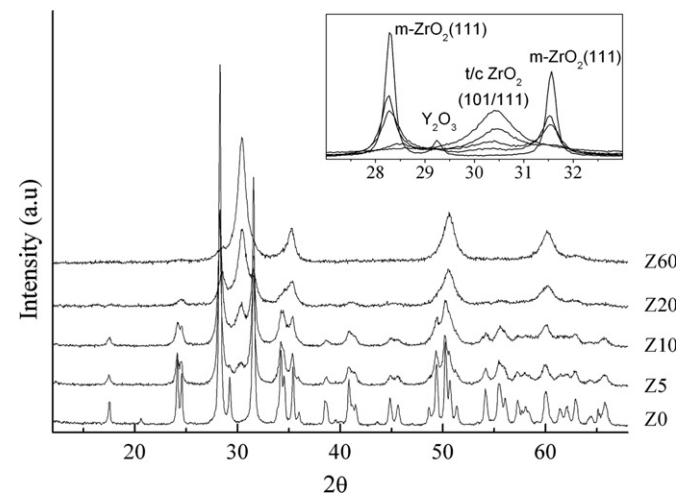

Fig. 1. X-ray diffraction patterns obtained after different milling times. The detail show clearly the rising of the tetragonal/cubic ZrO_2 (1 0 1) peak.

Table 1
Empiric XRD quantifications of the zirconia phases. And estimated SS lattice parameters (XRD–Rietveld).

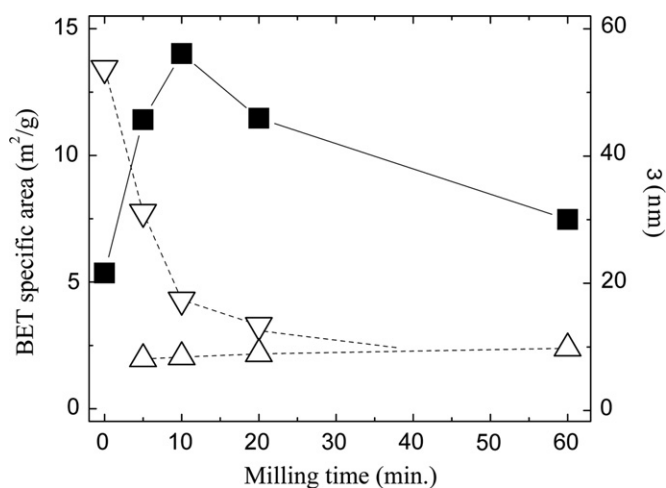| Milling time	m-ZrO$_2$ (Toroya)	%SS (Toroya)	$a \times \sqrt{2}$	c
0	100	0	–	–
5	97	3	50,923	52,036
10	91	9	50,892	52,077
20	39	61	50,953	51,870
60	0	100	50,758	51,530

Fig. 2. Results obtained for the BET specific area (black squares) and crystallite size (ε) deduced from the line widths for the monoclinic zirconia (empty triangle) and the tetragonal/cubic stabilized SS (clack triangle); tetragonal/cubic ZrO$_2$ solid solution content (SS) evaluated by XRD (black circles) as a function of the milling time. Lines are used to guide the eye.

Fig. 3. Spin rotation curves determined by PAC after different milling times. Solid lines represent the fit to obtain the quadrupole parameters ω_Q, η and δ as well as their relative fractions of the different quadrupole interactions.

remains almost steady at around 10 nm all over the milling time range.

The lattice parameters were estimated from a Rietveld refinement of the whole diffraction patterns and shown in Table 1. For short milling times (5 and 10 min) the c value was 0.520 nm which corresponds to an Y$_2$O$_3$ free or low Yttrium concentration tetragonal zirconia [30]. Besides, this parameter diminishes to 0.518 nm and 0.515 nm for the longer milling powders; the values are similar to the ones obtained by an Yttrium doped tetragonal zirconia. These facts suggest that for short mechanical treatment the observed SS is formed as a consequence of achieving the critical crystallite size and not due to the Yttrium substitutions, which occurs at long time treatments. On the contrary, the values evaluated for the $a \times \sqrt{2}$ product for all the milled samples correspond to a non-doped or low Yttrium concentration tetragonal zirconia [30], thus (being necessary) a more accurate phase characterization becomes necessary. The PAC technique permitted to identify and quantify the actual phase evolution. The results are shown in the following section.

3.1. PAC phase characterization and quantification

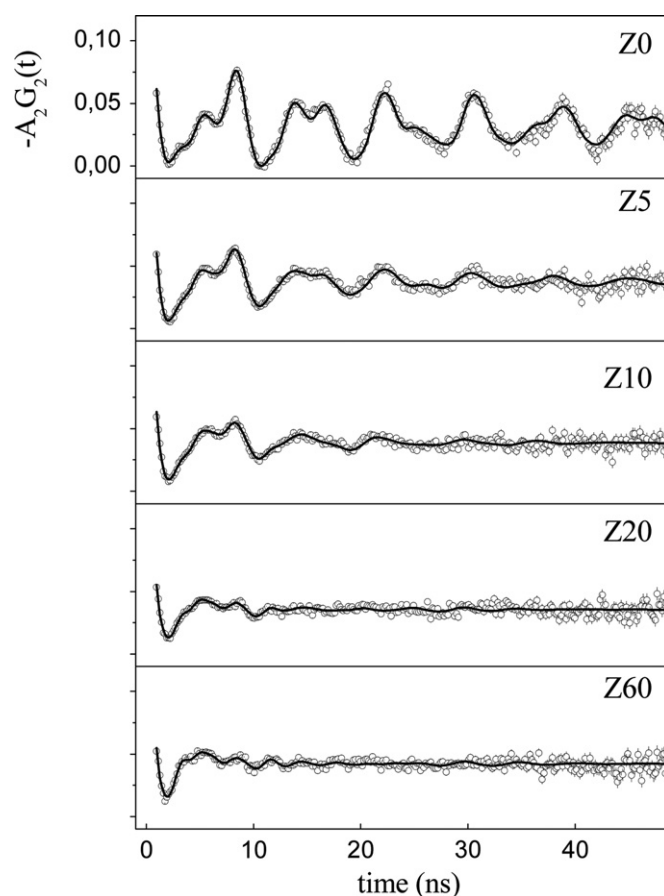Fig. 3 shows the spin rotation curves $A_2G_2(t)$ obtained from PAC experiments. In Fig. 4, the behavior of the quadrupole parameters determined via the fitting procedure is shown. No matter the milling time, the whole quadrupole interaction was a combination of three contributions I_1, I_2 and I_3, already reported to exist in zirconia and/or stabilized zirconias (see Table 2):

I_1 – The very well known hyperfine interaction describing crystalline monoclinic phase of ZrO$_2$ [31].

I_2 – Quadrupole interaction (m′-ZrO$_2$) similar but more assymetric and distributed than that of the crystalline monoclinic ZrO$_2$. This interaction, associated to distorted monoclinic zirconia, was reported to exist in milled pure ZrO$_2$ [25].

I_3 – Already known quadrupole interaction depicting the metastable tetragonal t'-phase of the ZrO$_2$. It was

reported to appear as a consequence of the charge compensation when dopping zirconia with aliovalen oxides [32] as well as by milling pure zirconia [25].

The relative fractions corresponding to the interactions I_1, I_2 and I_3 are shown in Table 3 as a function of the milling time.
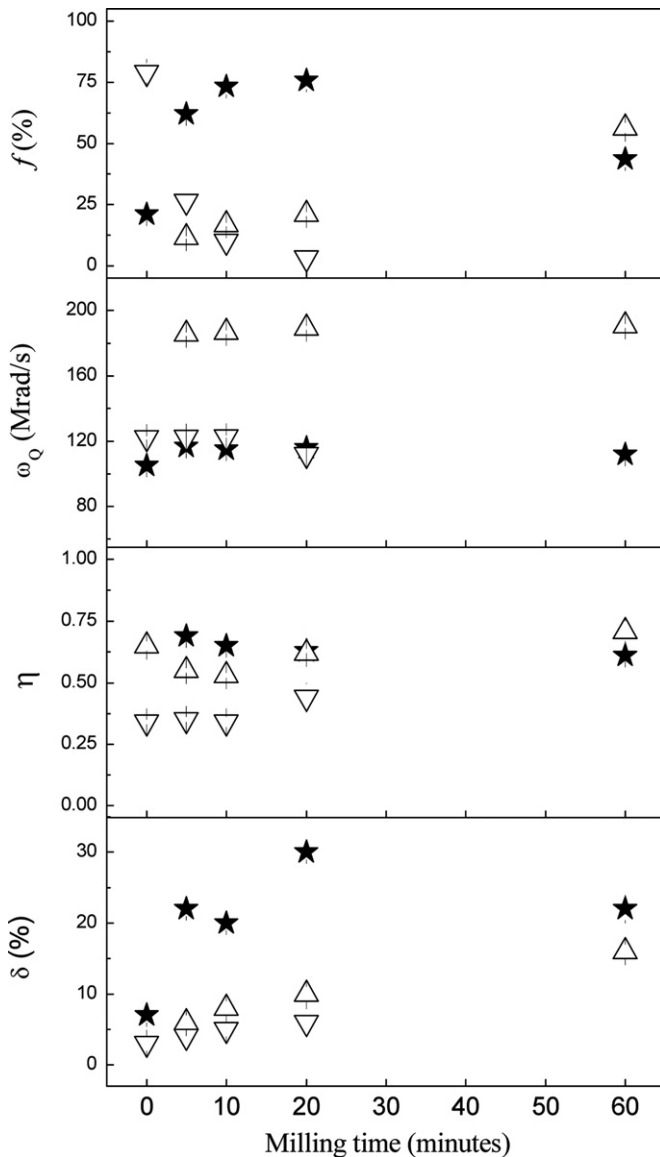

Fig. 4. Quadrupole parameters obtained after different milling times. Down triangles were used for monoclinic ZrO₂. Up triangles represent the interaction determined for a stabilized tetragonal SS and stars indicates the evolution of the distorted monoclinic form of ZrO₂.

It is clear that the starting sample Z0 is not a pure monoclinic zirconia despite the long range XRD result. Instead, the short range PAC technique shows the presence of a small amount of distorted configuration m′-ZrO₂ (interaction I_2). A consequence of the first 5 min of milling is observed: an important increase of the relative fraction of the distorted m cons₂ at the expenses of the one of m-ZrO₂ and the appearing of the $t'$and t interaction of ZrO₂. This last fact together with the XRD result for Z5 (disappearance of the main XRD peak of Y₂O₃ and the rising of a wide peak centered at about $2\theta = 29.24$) can be only interpreted as the formation of the tetragonal (ZrO₂)₀.₉₇(Y₂O₃)₀.₀₃ SS. PAC results indicate also that after 60 min of milling the amount of SS grows up to 56% being accompanied by distorted monoclinic zirconia (m′-ZrO₂).

As already reported by Scian et al. [25] the milling of pure monoclinic zirconia, in very similar conditions as the ones of the present experiments, stabilizes the tetragonal t'-form after more than 40 min of milling time. PAC signals of a widely distributed hyperfine interaction of t'-ZrO₂ (which indicates no crystalline material) is determined at 40 min of milling with no XRD manifestation. If those results are taken as a control experiment to check the effects to include Y₂O₃ during the milling process, it comes up that yttria clearly favors the formation of a more crystalline t'-form of ZrO₂ at shorter times.

The time evolution of the relative PAC fractions (see Fig. 4) suggest that during the HEM process the sequence of reactions m-ZrO₂→m′-ZrO₂→t'-ZrO₂ has occurred. If the PAC relative fractions play the role of concentrations of the different species in a solid material, the time evolution of the relative fractions can be obtained through a consecutive first order reactions mechanism:

$$m\text{-ZrO}_2 \overset{k_1}{\Rightarrow} \text{m}'\text{-ZrO}_2 \overset{k_2}{\Rightarrow} t'\text{-ZrO}_{2(\text{SS})} \tag{6}$$
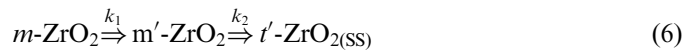
Table 3
Relative fractions determined by PAC representing the phase content evolution of the samples while milling. Experimental errors are between brackets.

Milling time	m-ZrO₂	m′-ZrO₂	t'-ZrO₂
0	79(4)	21(1)	0
5	26(2)	62(2)	12(1)
10	10(1)	73(3)	17(1)
20	3(1)	76(4)	21(1)
60	0	44(3)	56(2)

Table 2
Typical values of the quadrupole hyperfine parameters of the interactions determined in all the samples.

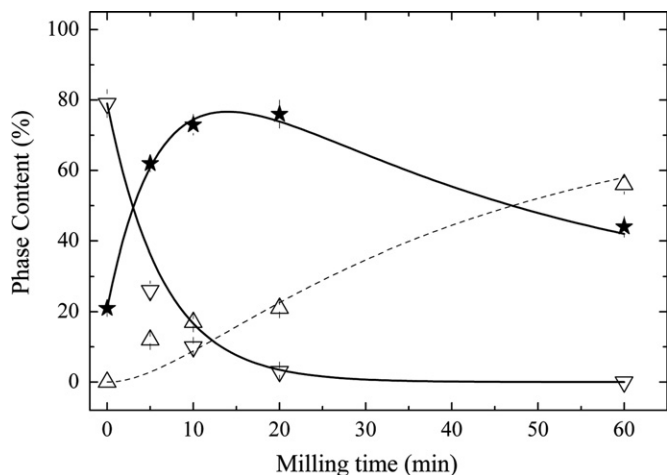| Interactions	ω_Q (Mrad/s)	η	δ(%)	Comments
I_1 m-ZrO₂	122	0.34	3	Well known interaction describing the monoclinic phase of ZrO₂ [28].
I_2 m′-ZrO₂	115	0.55	20	Quadrupole parameters reported to describe the distorted monoclinic form of ZrO₂ [25].
I_3 t'-ZrO₂	185	0.68	9	Quadrupole parameters depicting the tetragonal defective t'-form stabilized by charge compensation [29].

Fig. 5. Evolution of the relative fractions determined by PAC representing the charges in the phase content of the sample after different milling times. Symbols are the experimental results for the monoclinic phase (down triangles), the distorted monoclinic form (stars) and the stabilized tetragonal SS (up triangles). Curves display the corresponding predicted values deduced from the fitted rate constants.

whose solutions are

$$[m\text{-}ZrO_2] = [m\text{-}ZrO_2]_0 \exp(-k_1 t) \tag{7}$$

$$[m'\text{-}ZrO_2] = [m'\text{-}ZrO_2]_0 + \frac{k_1[m\text{-}ZrO_2]_0}{k_2 - k_1}(\exp(-k_1 t) - \exp(-k_2 t)) \tag{8}$$

$$[t'\text{-}ZrO_2] = [t'\text{-}ZrO_2]_0 + [m\text{-}ZrO_2]_0 \left(1 - \frac{k_2}{k_2 - k_1}\exp(-k_1 t)\right.$$
$$\left. - \frac{k_1}{k_2 - k_1}\exp(-k_2 t)\right) \tag{9}$$

The rate constants $k_1 = (0.16 \pm 0.02)$ min^{-1} and $k_2 = (0.025 \pm 0.003)$ min^{-1} were obtained by a least squares fitting procedure. Fig. 5 shows the comparison of the experimental values and the fitted curves.

The goodness of fit shows that the proposed mechanism is appropriate and it can be concluded that the mechanism is controlled by the tetragonal formation from the distorted monoclinic phase.

4. Conclusions/summary

Considering the results of long and short range techniques as XRD and PAC, the effects of HEM on ZrO_2–3%Y_2O_3 have been characterized.

- Nanocrystalline $(ZrO_2)_{0.97}(Y_2O_3)_{0.03}$ tetragonal solid solution powders were obtained directly from the high energy milling on stoichiometric mixtures of the pure oxides at room temperature.
- The XRD analysis evidenced the abrupt decrease of the crystallite size of monoclinic ZrO_2 from 55 to 15 nm during the first 10 min of milling. The fact is observed together with the appearance of the SS having 10 nm of crystallite size.

- Even when on one side XRD results show the evolution of the system from monoclinic ZrO_2 to SS, on the other side, PAC allows to establish that the distorted monoclinic m′-ZrO_2 phase plays the role of an intermediate in the SS formation which is tetragonal.
- The resulting Zr–Y–O solid solution corresponds to a not fully crystalline tetragonal phase.
- The time evolution of the phase content during HEM determined by PAC, clearly suggests the SS formation via the distorted monoclinic ZrO_2 phase is a consecutive first order reactions mechanism controlled by the reaction m′-ZrO_2 → t-SS.

Acknowledgements

References

[1] R.C. Garvie, The occurrence of metastable tetragonal zirconia as a crystallite size effect, Journal of Physical Chemistry 69 (1965) 1238–1243.

[2] R.C. Garvie, Stabilization of the tetragonal structure in zirconia microcrystals, Journal of Physical Chemistry 82 (1978) 218–224.

[3] T. Mitsuhasi, M. Ichihara, U. Tatsuke, Characterization, and stabilization of metastable tetragonal ZrO_2, Journal of the American Ceramic Society 57 (1974) 97–101.

[4] R. Cypres, R. Wollast, J. Raucq, Contribution on the polymorphic conversion of pure zirconia, Berichte der Deutschen Keramischen Gesellschaft 40 (1963) 527–532.

[5] J. Livage, K. Doi, C. Mazieres, Nature and thermal evolution of amorphous hydrated zirconium oxide, Journal of the American Ceramic Society 51 (1968) 349–353.

[6] J. Torralvo, M.A. Alario, J. Soria, Crystallization behavior of zirconium oxide gels, Journal of Catalysis 86 (1984) 473–476.

[7] G. Štefanić, S. Musić, A. Gajović, A comparative study of the influence of milling media on the structural and microstructural changes in monoclinic $ZrO2$, Journal of the European Ceramic Society 27 (2–3) (2007) 1001–1016.

[8] M.C. Fuertes, J.M. Porto López, Mechanochemical synthesis and thermal evolution of La^{3+}–ZrO_2 cubic solid solutions, Ceramics International 30 (2004) 2137–2142.

[9] G. Ye, T. Troczynski, Mechanical activation of heterogeneous sol–gel precursors for synthesis of $MgAl_2O_4$ spinel, Journal of the American Ceramic Society 88 (10) (2005) 2970–2974.

[10] G. Ye, T. Troczynski, Mechanochemical activation-assisted low-temperature synthesis of $CaZrO_3$, Journal of the American Ceramic Society 90 (1) (2007) 287–290.

[11] T.G. Shen, C.C. Koch, T.L. McCormick, R.J. Nemanich, J.Y. Huang, J.G. Huang, The structure and properties of amorphous/nanocrystallite silicon produced by ball milling, Journal of Materials Research 10 (1995) 139–148.

[12] T. Tsuchida, K. Horigome, The effect of milling on the thermal decomposition of alumina monohydrates, a- and b-Al_2O_3 _H_2O, Thermochimica Acta 254 (1995) 359–370.

[13] C.C. Yong, J. Wang, Mechanical-activation-triggered gibbsiteto–boehmite transition and activation-derived alumina powders, Journal of the American Ceramic Society 84 (6) (2001) 1225–1230.

[14] J. Temmujin, K.J.D. MacKenzie, M. Schmucker, H. Schneider, J. McManus, S. Wimperis, Phase evolution in mechanically treated mixtures of kaolinite and alumina hydrates (gibbsite and boehmite), Journal of the European Ceramic Society 20 (2000) 413–423.

[15] T. Tsuzuki, P.G. McCormick, Mechanochemical synthesis of nano-particles, Journal of Materials Science 39 (16–17) (2004) 5143–5146.

[16] J. Hernandez, J. Zarate, G. Rosas, Zirconia stabilization assisted by high energy ball-Milling, Journal of Ceramic Processing Research 10 (2) (2009) 144–147.

[17] A.C. Dodd, T. Tsuzuki, P.G. McCormick, Nanocrystalline zirconia powders synthesised by mechanochemical processing, Materials Science and Engineering A 301 (1) (2001) 54–58 15 March.

[18] A. Ghosh, A.K. Suri, B.T. Rao, T.R. Ramamohan, Low-temperature sintering and mechanical property evaluation of nanocrystalline 8 mol% yttria fully stabilized zirconia, Journal of the American Ceramic Society 90 (7) (2007) 2015–2023.

[19] J. Ding, T. Tsuzuki, P.G. McCormick, Mechanochemical synthesis of ultrafine ZrO_2 powder, Nanostructured Materials 8 (1) (1997) 7581.

[20] Françoise Daniel Michel, Eric Faudot, Léo Gaffet, Mazerolles, stabilized, zirconias prepared by mechanical alloying, Journal of the American Ceramic Society 76 (11) (1993) 2884–2888.

[21] N.M. Rendtorff, G. Suárez, Y. Sakka E.F. Aglietti, "Mechanochemical stabilization and sintering of nanocrystalline $(ZrO_2)_{0.97}(Y_2O_3)_{0.03}$ solid solution from pure oxides". IOP Conference Series: Materail Science and Engineering 18 (2011) 062018. 10.1088/1757-899X/18/6/062018.

[22] F. Farges, The structure of metamict zircon: a temperature-dependent EXAFS study, Physics and Chemistry of Minerals 20 (1994) 504–514.

[23] N.M. Rendtorff, M.S. Conconi, E.F. Aglietti, C.Y. Chain, A.F. Pasquevich, P.C. Rivas, J.A. Martínez, M.C. Caracoche, Phase quantification of mullite-zirconia and zircon commercial powders using PAC and XRD techniques, Hyperfine Interactions 198 (1) (2010) 211–218.

[24] M.C. Caracoche, J.A. Martínez, P.C. Rivas, M.A. Taylor, A.F. Pasquevich, S. Barolin, O.A. de Santis, Nanostructures in calcia stabilized hafnia thin films observed by PAC as a function of temperature, Hyperfine Interactions 179 (2007) 87–93.

[25] N. Scian, F. Aglietti, C. Caracoche, C. Rivas, F. Pasquevich, Lopez Garcia, R. Alberto, Phase transformations in monoclinic zirconia caused by milling and subsequent annealing, Journal of the American Ceramic Society 77 (6) (1994) 1525–1530.

[26] H. Toroya, M. Yoshimura, S. Somiya, Calibration curve for quantitative analysis of the monoclinic-tetragonal ZrO_2 system by X-ray diffraction, Journal of the American Ceramic Society 67 (1984) C119–C121.

[27] Rodriguez-Carvajal, J. Fullprof: A program for Rietveld refinement and pattern matching analysis (1990) Abstracts of the Satellite Meeting on Powder Diffraction of the XV Congress of the IUCr, pp. 127–128.

[28] H.M. Rietveld, A profile refinement method for nuclear and magnetic structures, Journal of Applied Crystallography 2 (1969) 65–71.

[29] H. Frauenfelder, R.M. Steffen, Angular Correlation, in: K. Siegbahn (Ed.), Alpha-, Beta- and Gamma-Ray Spectroscopy, North Holland, Amsterdam, 1965, p. 997.

[30] H.G. Scott, Phase relationships in the zirconia–yttria system, Journal of Materials Science 10 (9) (1975) 1527–1535.

[31] M.C. Caracoche, M.T. Dova, A.R. López García, J.A. Martínez, P.C. Rivas, Hyperfine interaction of ZrO_2—tetragonal phase, Hyperfine Interactions 39 (1988) 117–121.

[32] M.C. Caracoche, J.A. Martínez, A.F. Pasquevich, P.C. Rivas, E. DJurado, F. Boulc'h, PAC characterization of Gd and Y doped nanostructure zirconia solid solution, Physica B: Condensed Matter 389 (2007) 98–102.